



Ecosystem leaf area, gross primary production, and evapotranspiration responses to wildfire in the Columbia River basin

Mingjie Shi¹, Nate McDowell^{1,2}, Huilin Huang¹, Faria Zahura¹, Lingcheng Li¹, and Xingyuan Chen¹

¹Atmospheric, Climate, and Earth Sciences Division, Pacific Northwest National Laboratory, Richland, Washington, USA

²School of Biological Sciences, Washington State University, Pullman, Washington, USA

Correspondence: Mingjie Shi (mingjie.shi@pnnl.gov)

Received: 16 July 2024 – Discussion started: 26 July 2024

Revised: 21 January 2025 – Accepted: 29 January 2025 – Published: 9 May 2025

Abstract. Wildfires impact vegetation mortality and productivity and are increasing in intensity, frequency, and spatial area in the western United States. The rates of vegetation recovery after fires play a major role in the reestablishment of biomass and ecosystem functioning (e.g., structure, resilience, and productivity), but such recovery rates are poorly understood. Here we use remotely sensed data products from the Moderate Resolution Imaging Spectroradiometer (MODIS) to quantify the resistance and resilience of leaf area index (LAI), gross primary production (GPP), and evapotranspiration (ET) to 138 wildfires of various burn severity across the Columbia River basin (CRB) of the Pacific Northwest in 2015. Increasing burn severity caused lower resistance and resilience for all three variables. Resistance and resilience are highest in grasslands, intermediate in savanna, and lowest in needleleaf evergreen forests, consistent with the adaptation of these vegetation types to fire. LAI has consistently lower resistance and resilience than GPP and ET, which is consistent with physical and physiological mechanisms that compensate for reduced LAI. Resilience is influenced by precipitation, vapor pressure deficit (VPD), and burn severity across all three vegetation types; however, burn severity plays a more minor role in grasslands. Increasing wildfire severity will reduce the resistance and resilience and lengthen the recovery time of vegetation structure and fluxes with climate change, with significant consequences for the provision of ecosystem functioning and implications for model predictions.

1 Introduction

While agricultural activity changes reduce the global burned area (Andela et al., 2017), climate change increases the frequency and severity of wildfires (Burton et al., 2024; Jones et al., 2020; Pechony and Shindell, 2010). The western United States is experiencing increasing numbers of fire events, with the growth in burned areas and number of severe fires over the past 40 years (Juang et al., 2022; Parks and Abatzoglou, 2020; Schoennagel et al., 2017; Westerling, 2016). Wildfires cause large impacts on ecosystem carbon and water cycles that last for decades (Adams et al., 2012; Bart et al., 2020). They change ecosystem structure and species composition, and they modify soil properties, resource availability, the energy budget, and carbon storage (Anderegg et al., 2022; Bart et al., 2020; Lasslop et al., 2020; Turner, 2010). These changes manifest in vegetation-driven hydrologic changes in evaporation, transpiration, canopy interception, and they indirectly alter infiltration, runoff, groundwater recharge, and streamflow (Adams et al., 2012; Partington et al., 2022). The ecohydrological impacts of wildfires are expected to increase due to the consistently observed (Williams et al., 2019) and predicted (Rammer et al., 2021; Wimberly and Liu, 2014) increase in wildfire frequency and severity under climate change.

A primary mechanism underlying the ecohydrologic changes from wildfire is the loss of ecosystem-scale leaf area i.e., leaf area index (LAI) (Shrestha et al., 2024), that reduces gross primary production (GPP) and evapotranspiration (ET) through the loss of photosynthetic and transpiring surface area and microclimate shifts (Collar et al., 2021; Li et al.,

2018; Hu et al., 2008). The scale changes in LAI, GPP, and ET cascade down to numerous consequences, including reduced carbon storage and altered streamflow (McDowell et al., 2023; Seidl et al., 2014). Regional studies indicate that fire severity and post-fire plant community composition are essential to the spatial and temporal variations in ET (Collar et al., 2021; Poulos et al., 2021), where GPP and ET are tightly coupled in determining the ecohydrological processes (McDowell et al., 2023).

Resistance and resilience are the two metrics broadly used in ecology to evaluate recovery after disturbances. Resistance represents the ability of an ecosystem to withstand disturbance, while resilience represents the capacity of a system to recover its structure and function after a disturbance (Holling, 1973). Previous studies have used ecosystem traits, such as diameter at breast height, canopy height, live saplings (Proença et al., 2010), individual survival in fire, and pre- and post-fire bark thickness (Rodman et al., 2021), to estimate resistance and resilience due to fire-induced disturbance in forest plots. Wu and Liang (2020) explore both fire- and drought-determined resilience using two LAI products in different biomes at the global scale, suggesting the highest resilience in evergreen broadleaf forest. A study based on the continental United States implies that higher burn severities are consistently correlated with greater reductions in the ET-to-precipitation ratio (ET/P), while the biggest magnitude of ET changes and percent of ET/P reductions often occur in evergreen forests and in shrublands (Collar et al., 2021). Using the Moderate Resolution Imaging Spectroradiometer (MODIS) GPP product, a Hurricane Rita-based study suggests the difference in GPP recovery rates and resilience index between different vegetation types (Frazier et al., 2013). All these studies provide profound insights into disturbance impacts on ecosystem changes and regrowth (Albrich et al., 2020; DeSoto et al., 2020), implying that different vegetation types (VTs) may have different resistance and resilience determined by various disturbance intensity.

There have also been studies on the ecosystem-scale impacts and recovery of wildfires by using several different variables characterizing the ecosystem features (Jin et al., 2012; Mills et al., 2015). For example, a boreal-forest-based study indicates that aboveground biomass recovers more slowly than LAI and GPP, while GPP recovers more quickly than LAI (Yu et al., 2023). Using different MODIS products, Marcos et al. (2023) show that vegetation and soil water content has a higher resistance but slower and more gradual recoveries than production. In general, the recovery processes can be regulated by post-fire environmental conditions. For example, using a predictive machine learning model of time to recover, Rifai et al. (2024) reveal that the leaf area recovery of forests is strongly accelerated by a high post-fire precipitation anomaly. Currently, the immediate change and post-fire recovery of different ecosystem features (i.e., LAI, GPP, and ET) caused by the same fire events and their interactions with various burn severities (e.g., different burn severity cat-

egories; Eidenshink et al., 2007) have not been thoroughly quantified and compared, particularly at large scales (e.g., in river basins). Furthermore, the influence of environmental factors on post-fire ecosystem recovery, as characterized by LAI, GPP, and ET, remains inadequately quantified. This lack of clarity is closely linked to the uncertainties in predictions made by Earth system models (ESMs; Lawrence et al., 2016). Thus, it is essential to evaluate the post-fire carbon and water fluxes, which are essential to ecosystem recovery (i.e., returning to pre-fire carbon storage levels; Sun et al., 2020) and water resources (e.g., transpiration, streamflow; McDowell et al., 2023), respectively. An improved understanding of LAI, GPP, and ET responses to wildfire can benefit ESMs in term of reducing prediction uncertainties of wildfire impacts on the carbon and water cycles.

This study aims to comprehensively investigate the post-fire ecosystem features (e.g., canopy carbon status versus the carbon and water fluxes) characterized by resistance and resilience in the featured VTs of the Columbia River basin (CRB) across 138 fires with different burn severities in 2015. Previous studies document the findings regarding the different recovery features between VTs (DeSoto et al., 2020), the varied recovery features characterized by different variables (e.g., LAI, GPP, and ET) (Marcos et al., 2023; Yu et al., 2023), and the different responses of GPP to various environmental factors across VTs (Lu and Yan, 2023). Based on the existing research, we plan to test four research hypotheses: (1) higher burn severity results in lower resistance and resilience represented by all the three metrics across all the VTs; (2) with the same burn severity, resistance and resilience are highest in grasslands, intermediate in savanna, and lowest in forests; (3) across all VTs, resistance and resilience are highest for GPP and ET and lowest for LAI, a key factor determining GPP (Saigusa et al., 2005); and (4) precipitation and vapor pressure deficit (VPD) are more important to the resilience in grassland than in other VTs.

To test these hypotheses, we use the MODIS LAI, GPP, and ET products to quantify fire-induced changes in resistance and resilience, and the random forest feature importance method (Breiman, 2001) is used to investigate climate (e.g., precipitation, VPD) dependency. Here, we simultaneously and quantitatively examine the responses of LAI, GPP, and ET to fire disturbances by applying the resistance and resilience quantification framework discussed in DeSoto et al. (2020) to the MODIS products in relation to burn severity and VTs (e.g., forests, savanna, and grasslands) across the CRB in the Pacific Northwest, USA. Given that the impacts of wildfires are expected to intensify in the CRB (Halofsky et al., 2020; Wimberly and Liu, 2014) and globally (Andela et al., 2017; Bowman et al., 2020; Jones et al., 2024), quantifying fire impacts is essential for both ecosystems and society. The research framework of this study can be broadly applied to quantify wildfire-induced ecosystem responses and evaluate the impacts of wildfires as revealed by different data products and represented by ESMs.

2 Methods

The analyses are performed at spatial resolutions of 500–1000 m, and our research time frame is 2011–2020, which is centered around the time of maximum fire occurrence in the CRB in 2015. We use (1) the MODIS land cover type (LCT; Sulla-Menashe and Friedl, 2018) to identify surface VTs; (2) the burn severity product from the Monitoring Trends in Burn Severity (MTBS) program to classify the location and severity of fires (Eidenshink et al., 2007); (3) the meteorological data from ECMWF Reanalysis Version 5 (ERA5) to quantify annual variation in climate (Hersbach et al., 2020); and (4) the MODIS LAI (Myneni et al., 2002), GPP, and ET products (Running et al., 2004) to assess the ecosystem resistance and resilience due to fire disturbance. To interpret the essential factors controlling the resilience of different VTs, the random forest feature importance method is used to assess the importance of precipitation, VPD, and burn severity to the resilience values in 2020 represented by LAI, GPP, and ET. All the data and scripts for data processing are publicly available in the Environmental System Science Data Infrastructure for a Virtual Ecosystem (ESS-DIVE) repository (Shi et al., 2025).

2.1 Characterizing surface vegetation types

In this research, we use the annual 500 m MODIS LCT dataset, MODIS MCD12Q1 version 6.1 (Sulla-Menashe and Friedl, 2018; Friedl and Sulla-Menashe, 2022), to identify the surface VT (Supplement Table S1). The VT map in 2015 shows that needleleaf evergreen forest (NEF), woody savanna (WDS), grassland (GL), and cropland (CL) are the four dominant vegetation cover types over the CRB (Fig. S1 in the Supplement), and we study the impacts of wildfire over the NEF, WDS, and GL VTs.

2.2 Identifying the 2015 fire events

We identify all the 2015 fire events in the CRB in order to have sufficient data pre- and post-fire for calculating resistance and resilience and because 2015 is an extreme fire year in this region. MTBS (since 1984) maps burn extent and severity across the United States (Eidenshink et al., 2007; Picotte et al., 2020). It includes all fires $\geq 4.05 \text{ km}^2$ in the western United States, where burn severity is quantified as a visible alteration of vegetation, dead biomass, and soil that occurs within a fire perimeter (Eidenshink et al., 2007). Changes in vegetation status and biomass resulting from fires were assessed using the Composite Burn Index (CBI). These changes are also correlated with remotely sensed estimates such as the differenced Normalized Burn Ratio (dNBR), a metric measuring the difference between pre- and post-fire NBR images (Eidenshink et al., 2007). The burn severity product from MTBS is widely used as a viable estimate of

burn severity within certain ecosystems in the United States (Cansler and McKenzie, 2012; Picotte et al., 2020).

The MTBS products include burn perimeters and burn severity, and we use the burn severity categories to identify fires and their features (e.g., burned area, burn severity) over the CRB. The MTBS mapping primarily relies on the differenced normalized burn ratio (dNBR) algorithm and Landsat imagery in the near-infrared and shortwave infrared bands (Eidenshink et al., 2007). The same dNBR algorithm is applied to different VTs. Differenced NBR images – where post-fire NBR is subtracted from pre-fire NBR – are known as dNBR images. These dNBR images illustrate fire-related changes, which are categorized into severity classes, providing an unbiased foundation for analyzing additional fire effects (Eidenshink et al., 2007). The MTBS data are at a 30 m spatial resolution and upscaled to the 500 m spatial resolution for the comparison with the MODIS data products (Table S1). MTBS employs different integers to indicate burn severity categories, with values ranging from 1 to 4 representing unburned, low, moderate, and high severity, respectively. Consequently, the upscaling processes using the area-average remapping method produce floating-point numbers. Here, the numbers and meanings of burn severity values before and after the regroup are in Table S2. Based on this regroup method, the fire events and their burn severity in the CRB are shown in Fig. S2. To identify the vegetation type where each fire event occurred, we apply the MTBS fire boundary (i.e., shape) files, which describe the perimeter of each fire event, to the VT map (Fig. S1). We use the dominant VT of each fire event, defined as the VT whose area accounts for more than 50 % of burned area for that event, to identify the representative landscape type of each fire event (Fig. S2b). This analysis aims to comprehend which VT(s) are predominantly affected by fire events across the CRB (Fig. S2b). However, to precisely estimate the resistance and resilience of different VTs, we explicitly consider the VTs and their changes characterized by LAI, GPP, and ET in each data pixel of each fire event (see more details in Sect. 2.4). During the fire season of 2015, 138 fire events are identified. In all these burned areas, we remove the areas that experienced fire in 2011–2014 or in 2016–2020; thus, our resistance and resilience calculations are not confounded by repeat fires.

2.3 Interannual climate

We quantify interannual climate throughout the study region to determine if our resistance and resilience estimates were influenced by climatic variation. Here, we use precipitation, surface air temperature, and vapor pressure deficit (VPD) from ERA5 (2011–2020; Hersbach et al., 2020). The dataset is originally at the 30 km spatial resolution, and we use the nearest-neighbor method to downscale the data to the 500 m spatial resolution to match the spatial resolutions of other datasets (e.g., MODIS) of this study. The 10-year mean pre-

precipitation and surface air temperature are shown in Fig. S3. We then use the MODIS LCT suggested VT and MTBS burn severity information in each 500 m data pixel to group precipitation, surface air temperature, and VPD within each fire-disturbed region to their respective VT and then averaged the grouped climate variables for each VT. The specific process is the same to the MODIS LAI, GPP, and ET grouping, and more details of this method are introduced in the data description of MODIS data products of LAI, GPP, and ET.

2.4 Quantifying LAI, GPP, and ET

We use the MODIS LAI product at the 4 d interval and 500 m spatial resolution (Myneni et al., 2002) and the MODIS GPP and ET products at the 8 d interval and 1000 m spatial resolution (Running et al., 2004), which was downscaled to the 500 m spatial resolution by using the nearest-neighbor method. To identify LAI, GPP, and ET changes among different VTs and burn severity categories, we apply the MTBS boundaries and MODIS LCT suggested VTs to the MODIS LAI, GPP, and ET products. To ensure the calculation accuracy, we evaluate the variations in these metrics by using MODIS VT pixels within the fire boundaries to group these variables based on VTs and calculated the means for the same VTs across all the fire boundaries. Specifically, within each MTBS fire boundary, the MODIS VT information for each data pixel is used to derive different VT-determined LAI, GPP, and ET changes in the corresponding MODIS data pixels (Table S1). We then average the LAI, GPP, and ET of the same VT and with the same burn severity across all the 500 m MODIS data pixels. As discussed above, ERA5 precipitation and temperature data are also grouped between different VTs by using this method. Thus, instead of considering the dominant VT in each fire boundary, we accurately perform the calculation, which could avoid the errors associated with the weights of each VT in different fire boundaries. All the abovementioned calculations are performed during 2011–2020.

2.5 LAI-, GPP-, and ET-based resistance and resilience calculations

Following DeSoto et al. (2020), we define resistance and resilience as

$$\text{resistance} = \frac{A_{2016}}{\overline{A_{2011-2014}}}, \quad (1)$$

$$\text{resilience} = \frac{\overline{A_{2017-2020}}}{\overline{A_{2011-2014}}}, \quad (2)$$

where A represents the ecohydrological variables, LAI, GPP, and ET, used in this study, and the specific years are indicated in Eqs. (1) and (2). We exclude 2015 values of LAI, GPP, or ET in the calculations because the fires happened mid-way through the growing season (Fig. S4); thus the 2015 values include both pre- and post-fire, making them inappropriate

for resistance and resilience calculations. Given that resilience could exhibit interannual variations due to climate variations (e.g., DeSoto et al., 2020), we also calculate resilience for each individual year for all the VTs with various burn severity levels. DeSoto et al. (2020) define recovery as the condition following a disturbance compared to the condition in the year when the disturbance occurred, which can be represented by the following equation:

$$\text{recovery} = \frac{\overline{A_{2017-2020}}}{A_{2016}}. \quad (3)$$

Thus, the primary distinction between resilience and recovery lies in the reference conditions: pre-fire versus the disturbed conditions. Resilience is defined as the capacity of a system to recover its structure and function after a disturbance (Holling, 1973). To ensure clarity in our discussions of recovery status, we use the term resilience throughout this study.

We use LAI, GPP, and ET observations from the growing season, which we defined as days with values larger than 30 % of the annual maximum. This threshold number can be tweaked (Shi et al., 2020), and we choose to use this value to avoid the MODIS data uncertainty during snow seasons and minimize data noises. To avoid any error associated with using only a single observation, we identify the annual peak value and then averaged that value with records from the previous and subsequent 8 d to generate the annual maximum value. This means that, for MODIS LAI, with the 4 d temporal resolution, we average five contiguous records centered around the peak value. For MODIS GPP and ET, with the 8 d temporal resolution, we average three records: one before the peak, the peak itself, and one after the peak. To obtain the start and end of the growing seasons, we calculate the four-record running mean (i.e., 16 d) of LAI and the two-record running mean (i.e., 16 d) of GPP and ET over the entire year. The start of each year's growing season is determined when the running mean exceeds 30 % of the annual maximum value, and the end of the growing season was calculated when the running mean dropped below 30 % of the annual maximum. The growing season length based on different vegetation types with varied burn severity is shown in Fig. S5.

2.6 Random forest feature importance

To interpret the factors controlling resilience of different VTs, the random forest feature importance method (Breiman, 2001) is implemented using the scikit-learn package in Python. Random forest uses a large collection of decision trees to predict the target variable based on its relationship with a specified set of input features. Each tree learns from a randomly chosen subset of samples and features, while the final prediction is made by averaging predictions from all trees. Furthermore, the algorithm reports the relative impor-

tance of input features by considering the reduction in impurity achieved by each feature during tree construction.

For this analysis, the random forest was trained with a set of input features that include burn severity in 2015 and total precipitation and mean VPD between 2017 and 2020 for each grid in the burned areas. Nine separate models were trained to predict three target variables: resilience for LAI, GPP, and ET in the year 2020 for NEF, WDS, and GL. The number of samples in NEF, WDS, and GL were 11 881, 15 684, and 26 840, respectively.

Random forest hyperparameters, such as the number of trees and number of features considered at splitting, were predefined before model training. Here, the number of trees was set to 100. The GridSearchCV algorithm from the scikit-learn package was applied to 85 % of randomly chosen samples to find the optimal number of features considered at splitting, and it was determined to be 1. Model training and testing were performed by splitting the samples randomly with 85 % in training and 15 % in testing. The random forest model was trained 100 times by performing 100 randomized splits to reduce any bias from splitting, where the experimental design with the model trained 100 times was well tested by previous studies (Juarez-Martinez et al., 2023; Sadler et al., 2018). From the 100 trained models, the distribution on train and test R^2 scores was obtained and the relative importance for each feature was averaged.

3 Results

3.1 The meteorological conditions and burn severity in the CRB

The MTBS- and VT-based analysis shows that August is the month with the highest fire frequency in 2015 with 91 fire events (Fig. S2a), where NEF experiences 42, WDS experiences 27, and grassland experiences 67 fire events, respectively (Figs. S1 and S2b). The northern CRB experiences a higher incidence of forest fires, whereas the southern CRB is mainly affected by grassland fires (Figs. S1, S2c, and S2c). There are two fire events in croplands, which were excluded from further analysis.

The mean precipitation and surface air temperature over the Columbia River basin are $789 \pm 63 \text{ mm yr}^{-1}$ and $5.7 \pm 0.7^\circ\text{C}$ during 2011–2020 (Fig. S3). The spatial pattern of precipitation and surface air temperature suggests relatively warmer and drier conditions in the southern part of the basin, where the areas are mostly covered by grassland (Fig. S1). The western and northeastern areas of the basin have higher precipitation, ranging from 700 to 1300 mm yr^{-1} , and lower air temperatures, ranging from -3.0 to 11.0°C (i.e., from the northernmost part to the central–southern part of the CRB; Fig. S3b). These areas have a greater proportion of NEF and WDS (Figs. S1 and S3). We further examine the climate for each of the 138 fire

locations broken into the three vegetation types. Climate conditions in 2015, the year of high fire activity, are particularly dry and warm across all vegetation types. There is no significant difference in mean annual precipitation and surface air temperature between 2011–2014 and 2016–2020 (Fig. S4 and Table S3). Therefore, climate variations are not confounding resistance and resilience calculations.

3.2 LAI, GPP, and ET 2011–2020

Wildfires reduce LAI, GPP, and ET below the pre-fire mean in all VTs at the highest burn severity (herein S_{burn} ; $S_{\text{burn}} > 3$; Fig. 1; we present results for S_{burn} below 3 in Fig. S7 and Table S2). The 2011–2014 growing season mean LAI values are 1.87 ± 0.10 , 1.47 ± 0.04 , and $1.16 \pm 0.03 \text{ m}^2 \text{ m}^{-2}$ over NEF, WDS, and GL, respectively. The growing season LAI has an increasing trend from 2016 to 2020 in all the VTs, with 2020 values of 1.18, 1.04, and $0.88 \text{ m}^2 \text{ m}^{-2}$ for NEF, WDS, and GL, respectively (Fig. 1a). GPP and ET patterns are similar to those of LAI, with the highest values during 2011–2014 and the lowest values in 2016. GPP and ET in 2020 are not back up to the mean 2011–2014 values (Fig. 1b and c). Similar but less dramatic declines in LAI, GPP, and ET are observed in the lower burn severity classes (Table S2 and Fig. S7). We also calculate the standard error across the burned pixels of each VT by using all three metrics, i.e., LAI, GPP, and ET (Figs. 1 and S7). The ratio between the standard error and the spatial mean is highest when $S_{\text{burn}} > 3$, and this ratio decreases with burn severity. This ratio also tends to decrease with ecosystem complexity, with the highest values in NEF and the lowest values in GL (figure not shown), and its ranges across the three VTs are 0.067–0.072 for LAI, 0.090–0.100 for GPP, and 0.067–0.80 for ET, respectively, where the lower bounds consistently represent the values for GL. These results indicate relatively high spatial variations in all the three metrics when burn severity increases, and, in the same burn severity category, the spatial variations in LAI are smaller than those in GPP and ET (Figs. 1 and S7).

3.3 LAI, GPP, and ET resistance and resilience to wildfire

We first present wildfire resistance and resilience for each VT (using Eqs. 1 and 2) across the burn severity categories and present the results as a function of time further below. Resistance to wildfire declines with increasing burn severity values for LAI, GPP, and ET, and it is highest for GL, intermediate for WDS, and lowest for NEF VTs, regardless of response parameter (i.e., LAI, GPP, or ET; Fig. 2a, c, and e). Resilience to wildfire, calculated as the average resilience value from 2017–2020, is lower with higher burn severity for LAI, GPP, and ET (Fig. 2b, d, and f). Like the patterns of resistance values, resilience is highest for GL, intermediate for WDS, and lowest for NEF. GL resilience is near 1 for all three variables in GL when burn severities are below 2.

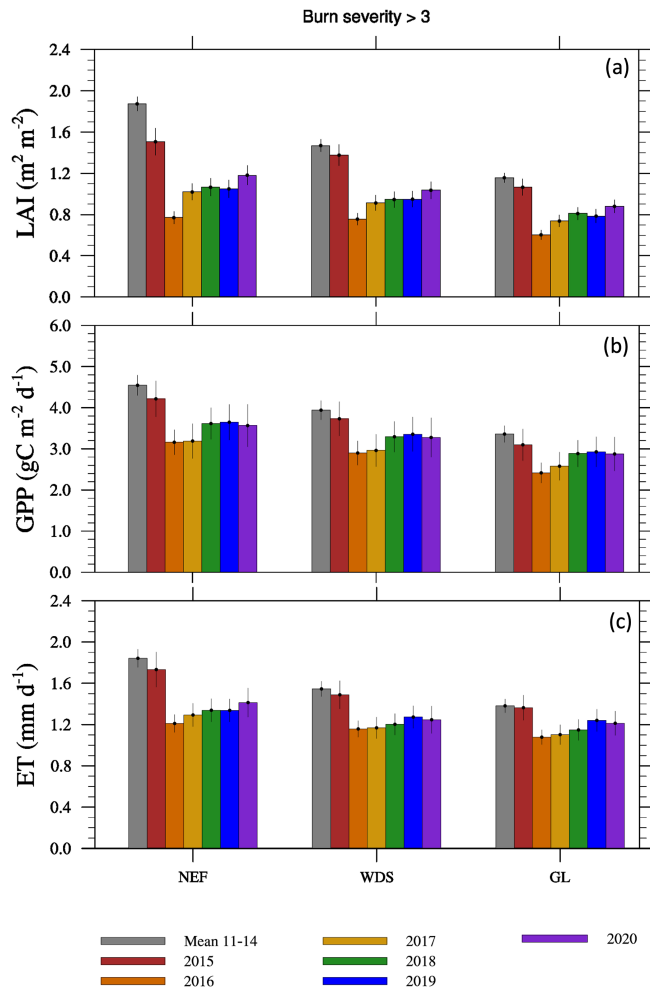


Figure 1. The growing season (a) LAI, (b) GPP, and (c) ET variation over needleleaf evergreen forests (NEF), woody savannas (WDS), and grasslands (GL) with burn severity > 3 during 2011–2020. See Fig. S7 for these results for fires with burn severities less than 3. The standard errors are included on the bars to represent the data variability across data pixels of different VTs.

Resistance and resilience calculated at the annual scale using Eqs. (1) and (2) show the responses of LAI, GPP, and ET relative to each other (Fig. 3; $S_{\text{burn}} > 3$ shown; S_{burn} values below 3 are shown in Figs. S8–S10). Within each VT, resistance and resilience are similar for GPP and ET and are lower for LAI. Resistance and resilience increase for all parameters with lower burn severities (Figs. S8–S10) and are lowest for NEF, intermediate for WDS, and highest for GL VTs. The standard errors obtained from the resistance and resilience values across different pixels indicate that LAI suggested resistance and resilience have relatively smaller spatial variations than those represented by GPP and ET. Given that resilience is closely related to water availability and burn severity (Fig. 4 and the description below), the resilience under the same burn severity shows similar interannual variability

(Fig. 3). Furthermore, the recovery capability (i.e., resilience) is similar for NEF and WDS when they are disturbed by the same burn severity (Fig. 3a and b).

To examine the drivers of the interannual variation in resilience characterized by LAI, GPP, and ET, we use the random forest feature importance method to identify the contributions of precipitation, VPD, and burn severity to influencing ecosystem resilience. Burn severity is more important for NEF and WDS VTs than for GLs (Fig. 4). In NEF, precipitation and VPD have importance scores of 0.3 for LAI resilience, while that of burn severity is 0.4 (Fig. 4a). Similarly, in WDS, the importance scores of precipitation and VPD are 0.28 and 0.29, while that of burn severity is 0.43 (Fig. 4b). Precipitation and VPD have relatively similar importance scores within VTs but were higher for GLs. In GL, the scores of precipitation, VPD, and burn severity to LAI-represented resilience are 0.43, 0.40, and 0.16, which shows the reduced importance of burn severity to GL. The importance scores for GPP- and ET-represented resilience show variations. However, the overall conclusion regarding the contributions of these three metrics to resilience values remains consistent across the VTs. The train and test scores of different resilience values are included in Fig. S11. The median R^2 scores for train and test datasets over 100 iterations ranged between 0.68–0.71 and 0.62–0.67, 0.61–0.66 and 0.54–0.61, and 0.57–0.68 and 0.57–0.64 for LAI, ET, and GPP, respectively, for the three VTs. As the median R^2 scores for train and test datasets are close, this suggests the model is not significantly overfitting and learning the underlying patterns in the dataset (Yang et al., 2024; Yildirim et al., 2021).

4 Discussion

This study examines the immediate impacts and subsequent recovery of vegetation to 138 CRB wildfires in 2015 with multiple burn severity levels by using remotely sensed metrics of LAI, GPP, and ET within a formal resistance and resilience framework (DeSoto et al., 2020). The random forest feature importance algorithm is used to quantify the contributions of different factors, i.e., precipitation, VPD, and burn severity, to resilience. This study quantitatively assesses the post-fire resistance and resilience determined by different MTBS burn severity categories in different VTs through simultaneously using the three MODIS products (i.e., LAI, GPP, and ET). Overall, resistance and resilience reductions are closely related to burn severity increase, which matters more to the forest VT. Resilience is influenced by precipitation, VPD, and burn severity across all three VTs; burn severity plays a more important role in the resilience of forest and savanna VTs, while precipitation and VPD are more essential to the resilience of grassland.

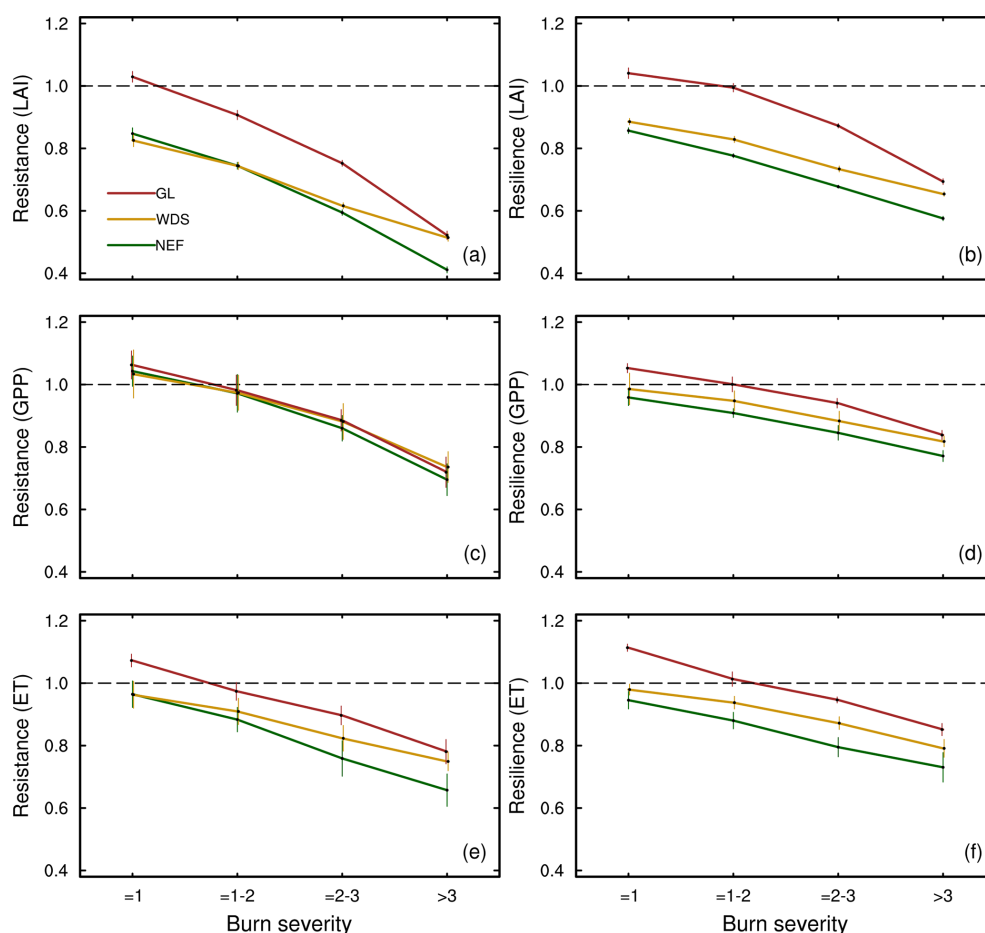


Figure 2. LAI (a) resistance and (b) resilience, GPP (c) resistance and (d) resilience, and ET (e) resistance and (f) resilience in needleleaf evergreen forests (NEF), woody savannas (WDS), and grasslands (GL) with different burn severities (Table S2). Resistance is calculated using the 2016 data. The 2016 resistances are the same as those shown for $S_{\text{burn}} > 3$ in Fig. 3 and are retained here to show the trends. The resilience calculation uses the mean of 2017–2020. The standard errors are included to represent the data variability across data pixels.

4.1 Burn severity controls on ecosystem recovery

In all the studied VTs with burn severity larger than 3, the ecosystem status (i.e., LAI) and fluxes (i.e., GPP and ET) did not recover to pre-fire conditions within the post-fire study period (Fig. 1). Figure 2 also shows that the increase in burn severity will reduce resistance and resilience across all the VTs, implying the lengthened recovery time of vegetation structure and fluxes. Among the three VTs, resistance and resilience are highest in grasslands, intermediate in woody savanna, and lowest in needleleaf forests. By exploring plant diversity and measured productivity across a variety of grassland sites in Europe and North America, Isbell et al. (2015) demonstrated full recovery 1 year after some drought disturbances. These trends can be attributed to the evolution of ecosystems to tolerate various disturbances, where grasslands are adapted to more frequent fires and droughts in part through resprouting from their extensive root systems and can regrow leaf area far more rapidly than forests (Ratajczak

et al., 2014; Isbell et al., 2015). These results support our first and second hypotheses that (1) higher burn severity results in lower resistance and resilience across all VTs and, (2) with the same burn severity, resistance and resilience are highest in grasslands, intermediate in savanna, and lowest in forests. Here, we estimate resistance by using the values of these three metrics in the first post-fire year (i.e., 2016) for all the VTs. When burn severity is 1, some ecosystems, such as grasslands, can recover rapidly, and the values in 2016 may exceed those in 2015 or in 2011–2014 (see Fig. S7). These variations (Fig. S7c, f, and i) are primarily influenced by the minimum disturbance intensity, which could facilitate a quick recovery under favorable climate conditions.

It has been suggested by previous studies that severe fires can induce VT changes and ecosystem degradation (e.g., Karavani et al., 2018; Kumar et al., 2024). To further investigate the role of VT changes in ecosystem resilience over the CRB, we apply the burn severity map (Fig. S2c) to both the 2014 and 2020 VT maps (i.e., the regions without fire dis-

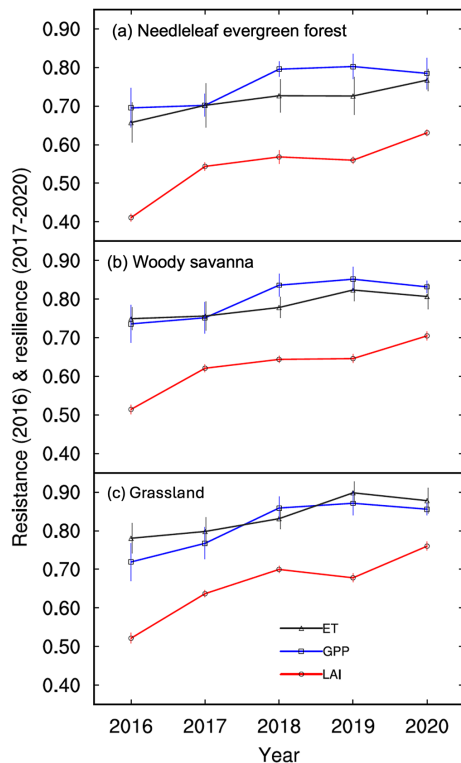


Figure 3. LAI, GPP, and ET temporal trends in wildfire resistance (2016) and resilience (years 2017–2020) for (a) needleleaf evergreen forests, (b) woody savannas, and (c) grasslands with burn severity (S_{burn}) larger than 3. The standard errors are included to represent the data variability across data pixels.

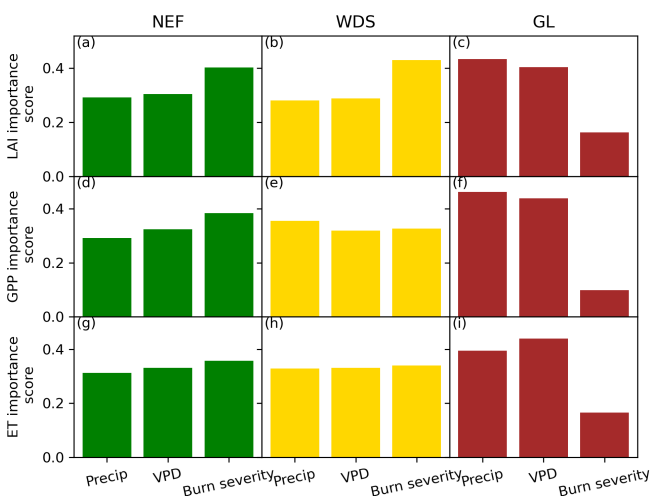


Figure 4. The feature importance of precipitation, VPD, and burn severity to resilience values in 2020 for LAI (a–c) NEF, WDS, and GL; GPP (d–f); and ET (g–i).

turbance are excluded), and the results show that, among the 67 090 fire-disturbed data pixels in the CRB, 13 363 (20 %) NEF, 7832 (12 %) WDS, and 706 (1 %) GL pixels experience VT changes (Figs. 5 and S12). In other words, most of the fire-disturbed pixels with VT changes contain woodlands. This finding further justified that grasslands are better adapted to wildfires (Isbell et al., 2015). Figure 2 shows that the resilience values of WDS are comparable to those of GL at high burn severities (i.e., $S_{\text{burn}} > 3$), while, at relatively low severities, they align more closely with those of NEF. Since WDS is an ecosystem that combines elements of woodland and grassland, this result implies that the grass component can recover quickly even under high burn severity, despite the potential damage to both trees and grass. Furthermore, it is shown by previous studies that it can take decades to over 100 years for the recovery of needleleaf trees (e.g., Turner et al., 2019). Thus, the existing observational time frame (e.g., until 2024) is not long enough for quantifying the forest recovery, and whether trees can grow back in NEF and WDS is uncertain. The low resilience values in Fig. 2, especially under high burn severity categories, could also be associated with fire-induced VT shifts (e.g., tree to grass). One possible scenario is that, in the next a few decades, NEF will regenerate, and the dominance of grass will decrease with the reestablishment of trees, which will compete with grassland for light and nutrients. This assumption can be tested by dynamic global vegetation models (DGVMs), such as the Energy Exascale Earth System Model Land Model (ELM-FATES; Koven et al., 2020), which can be used to perform long-term simulations. Thus, using DGVMs to further understand the post-fire vegetation dynamics in the CRB and other regions with similar climate conditions could be our future research direction.

4.2 The interactions between the carbon pools and ecosystem fluxes

In all the resistance and resilience calculations based on different MODIS products, LAI has the lowest resistance and resilience values, whereas GPP and ET have similar values (Fig. 3). In other words, structure (i.e., LAI, a proxy of canopy biomass) has lower resistance and resilience than ecosystem fluxes (i.e., GPP and ET). The results are consistent with the previous studies showing that forests tend to increase stomatal conductance and hydraulic efficiency, promoting the return of tree-scale transpiration after fires (Nolan et al., 2014). Cooper et al. (2019) also show the enhanced transpiration rates for forests with moderate burn severity. All these findings support the relatively quicker recovery of GPP and ET than that of LAI.

GPP is an indicator of “ecosystem wellness” (Frazier et al., 2013), and ET is a water budget component mostly sensitive to vegetation changes (DeBano et al., 1998). The resistance and resilience value differences (Figs. 1, 2, and 3) also show the different recovery features of these two variables

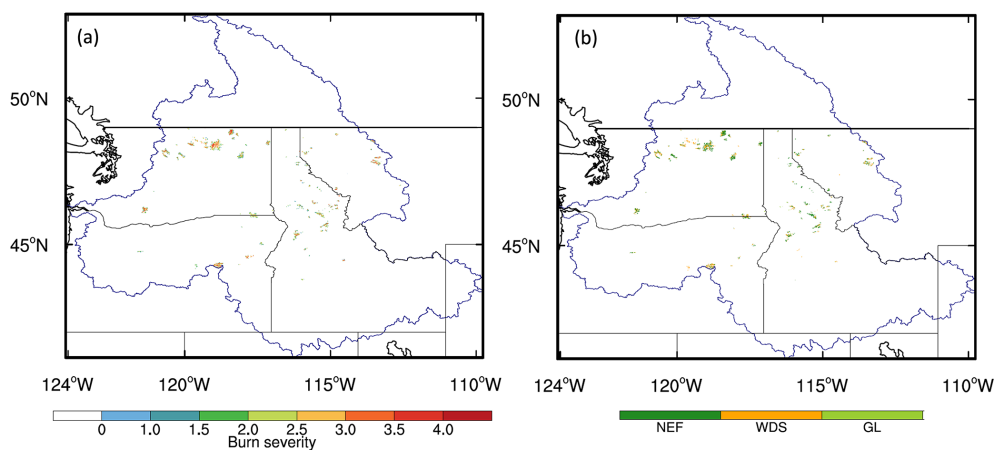


Figure 5. The spatial distribution of (a) the burn severity of data pixels experiencing the 2015 fires and (b) the pre-fire (i.e., 2014) VTs in the corresponding pixels of panel (a). NEF, WDS, and GL represent needleleaf evergreen forest, woody savanna, and grassland, respectively.

in various burn severities and VTs. We acknowledge that the MODIS GPP and ET products use the MODIS LAI and fraction of photosynthetically active radiation (fPAR) and the same meteorological data for their estimates (Running et al., 2004). Specifically, the MODIS GPP algorithm uses the following to estimate GPP: (1) the MODIS fraction of photosynthetically active radiation (fPAR) retrieved at the same time with LAI, (2) the MODIS daily mean photosynthetically active radiation (PAR), and (3) the biome-specific radiation use efficiency parameters that are extracted from the Biome Property Look-Up Table (BPLUT) and adjusted by the temperature and VPD scalars (Running and Zhao, 2019). The estimates of MODIS ET use the Penman–Monteith equation, which considers many environmental factors, including radiation components, air temperature, and relative humidity. Here, LAI is used to estimate wet canopy resistance to sensible heat and resistance to latent heat transfer, which will be used to calculate evaporation on wet canopy surfaces (Running et al., 2019). Thus, the recovery of GPP and ET are also affected by post-fire environmental factors, which do not respond to burn severity and have large daily, seasonal, and interannual variabilities. The similar responses of GPP and ET to fires could be associated with the tight coupling between these two fluxes, which is governed by stomatal conductance. Stomatal conductance regulates both photosynthesis and transpiration (Knauer et al., 2020; Stoy et al., 2019) and the correlations between GPP and ET (Running et al., 2004). Partitioning the contributions of GPP and ET coupling, and the methods used to derive GPP and ET data, is beyond the scope of this study. Here, our third hypothesis is supported, and it suggests that resistance and resilience are highest for GPP and ET and lowest for LAI across all VTs.

4.3 The environmental controls on resilience

It is shown by Lu and Yan (2023) that GPP can decrease with the increase in VPD in a grassland ecosystem, where this VPD limitation on GPP is not obviously shown in a nearby forest ecosystem. Since both precipitation and VPD largely influence vegetation growth in the semi-arid region, we explicitly test the fourth hypothesis to further understand the contributions of environmental factors (i.e., precipitation and VPD) and burn severity in determining the post-fire ecosystem recovery between VTs. The random forest feature importance study reveals that precipitation, VPD, and burn severity have various impacts on resilience represented by different variables across VTs. Even though burn severity is less important to grassland resilience (Fig. 4), the forest and savanna VTs show a stronger influence of burn severity on resilience in terms of LAI. Together, these results point to the interaction of precipitation, VPD, and burn severity in regulating ecosystem resilience and the higher and longer-lasting impacts of wildfires on VTs with higher biomass. The results also show that our fourth hypothesis, anticipating higher importance of precipitation and VPD to resilience in grassland than in other VTs, is testable. The post-disturbance biotic factor determining slow recovery of the forest ecosystems is also identified by Shi et al. (2017), who perform numerical simulations based on the 2005 Amazonian drought with the Community Land Model (CLM), revealing the limited influence of environmental factors to the forest recovery.

The random forest feature importance study implies that hydraulics are influenced almost equally by water supply (i.e., precipitation) and demand (i.e., VPD). Here, Figs. 1 and 3 show similar recovery trends across NEF, WDS, and GL, while Fig. 4 implies various importance scores of different factors in determining water dynamics and burn severity. We notice the differences in precipitation and temperature among these three VTs (Fig. S4), with relatively drier

and hotter conditions in GL, which underscores the role of climate in shaping the distribution of different VTs (Mather and Yoshioka, 1968). In other words, the importance scores highlight the roles of different factors in recovery across VTs, which adapt to specific environmental conditions (Figs. S1, S3, and S4) and exhibit their respective recovery rates. Advanced studies are needed to investigate the varied impacts of precipitation and VPD on resilience in different ecosystems with various types of disturbance (e.g., droughts and heat waves), which will further imply ecosystem recovery capacity and functionality shifts due to disturbance and is beyond the scope of this study. In addition, the post-fire interactions between LAI, GPP, and ET, and the sensitivity of these variables to burn severity and environmental factors during the recovery process, can be further evaluated by using ESMs. Research toward this direction can be used to guide model parameterization and enhance process-based representation in reasonably characterizing impacts of fires in different ecosystem types in ESMs.

4.4 Data uncertainty and application limitations

It is shown by previous studies that spectral observations of forests' canopy characteristics (e.g., leaf area) tend to be biased, resulting from clouds and aerosols along the measurement pathways (Asner and Alencar, 2010; Samanta et al., 2013; Xu et al., 2011). Therefore, the application of this research framework to other regions with fire disturbance, especially in the tropics with dense vegetation coverage, is limited by the observational capacity of spectral-based measurements. This also implies that intensified airborne measurements and lidar measurements can be extremely useful for enhancing the fundamental understanding of ecosystem processes after disturbances.

5 Conclusions

The results of this study suggest the decrease in resistance and resilience to burn severity increases and the higher resilience of grassland compared to forest and savanna VTs, which is largely regulated by precipitation and VPD during the recovery processes. Our research affirms the findings from plot-based measurements and shows a strong potential for using satellite observations to investigate ecohydrological processes and resistance and resilience to different types of disturbance in regions with reasonable data quality controls (i.e., with the remote-sensing quality control flags considered). The data revealed recovery feature differences between LAI, GPP, and ET and their variations between VTs, which, determined by varied burn severity, can largely be used to interpret fire-induced carbon and water cycle changes in terrestrial biosphere models (TBMs) and enhance the parameterization of models. The findings obtained from the random forest feature importance study can also be used to

guide sensitivity tests (e.g., precipitation perturbation tests) and advance physical-based understanding in TBMs.

With anticipated hotter and drier fire seasons with extended duration in the Pacific Northwest according to future climate projections (Wimberly and Liu, 2014), we expect that the fire frequency and burn severity of wildfires will increase with the changing climate patterns. This study implies that, with these changes, some ecosystems may need long time frames to achieve full recovery. This prolonged recovery could keep carbon stocks at relatively low levels for decades to 1 century (Turner et al., 2019) and affect the ecosystem function and ecosystem–atmosphere interactions (Harris et al., 2016). Thus, both data-oriented studies and the enhanced model capacity in reasonably predicting fire frequency and burn severity and properly characterizing impacts of fires in different ecosystem types are essential to the research of the carbon cycle, ecosystem functioning, and climate change.

Code and data availability. The data and code are publicly available in the ESS-DIVE repository under the Creative Commons Attribution 4.0 International License using <https://doi.org/10.15485/2507048> (Shi et al., 2025).

Supplement. The supplement related to this article is available online at <https://doi.org/10.5194/bg-22-2225-2025-supplement>.

Author contributions. MS, NM, and XC were responsible for conceptualization. MS and NM designed the study and wrote the first draft of the paper. HH prepared and processed the burn severity data, and LL provided the vegetation type data. MS worked on the remote-sensing data analysis and visualization, and FS performed the random forest feature importance tests. XC was responsible for funding acquisition. All the authors contributed to revising the article.

Competing interests. The contact author has declared that none of the authors has any competing interests.

Disclaimer. Any subjective views or opinions that might be expressed in the paper do not necessarily represent the views of the US Department of Energy or the United States Government.

Publisher's note: Copernicus Publications remains neutral with regard to jurisdictional claims made in the text, published maps, institutional affiliations, or any other geographical representation in this paper. While Copernicus Publications makes every effort to include appropriate place names, the final responsibility lies with the authors.

Acknowledgements. We would sincerely like to thank the two anonymous reviewers for their valuable comments and constructive

feedback, which greatly improved the quality of this work. This research was supported by the US Department of Energy (DOE) Office of Science (SC) Biological and Environmental Research (BER) program as part of BER's Environmental System Science (ESS) program. This contribution originates from the River Corridor Scientific Focus Area (SFA) and the Interoperable Design of Extreme-scale Application Software (IDEAS)–Watersheds project at Pacific Northwest National Laboratory (PNNL). PNNL is operated for DOE by Battelle Memorial Institute under grant no. DE-AC05-76RL01830. This research used resources of the National Energy Research Scientific Computing Center, a DOE Office of Science User Facility supported by the Office of Science of the US Department of Energy under grant no. DE-AC02-05CH11231, using an NERSC award (grant no. BER-ERCAP0023098).

Financial support. This research was supported by the US Department of Energy (DOE) Office of Science (SC) Biological and Environmental Research (BER) program as part of BER's Environmental System Science (ESS) program.

Review statement. This paper was edited by Andrew Feldman and reviewed by two anonymous referees.

References

- Adams, H. D., Luce, C. H., Breshears, D. D., Allen, C. D., Weiler, M., Hale, V. C., Smith, A. M., and Huxman, T. E.: Ecophysiological consequences of drought-and infestation-triggered tree die-off: insights and hypotheses, *Ecophysiology*, 5, 145–159, <https://doi.org/10.1002/eco.233>, 2012.
- Albrich, K., Rammer, W., Turner, M. G., Ratajczak, Z., Brazunas, K. H., Hansen, W. D., and Seidl, R.: Simulating forest resilience: A review, *Global Ecol. Biogeogr.*, 29, 2082–2096, <https://doi.org/10.1111/geb.13197>, 2020.
- Andela, N., Morton, D. C., Giglio, L., Chen, Y., van der Werf, G. R., Kasibhatla, P. S., DeFries, R. S., Collatz, G. J., Hantson, S., Kloster, S., and Bachelet, D.: A human-driven decline in global burned area, *Science*, 356, 1356–1362, <https://doi.org/10.1126/science.aal4108>, 2017.
- Anderegg, W. R., Wu, C., Acil, N., Carvalhais, N., Pugh, T. A., Sadler, J. P., and Seidl, R.: A climate risk analysis of Earth's forests in the 21st century, *Science*, 377, 1099–1103, <https://doi.org/10.1126/science.abp9723>, 2022.
- Asner, G. P. and Alencar, A.: Drought impacts on the Amazon forest: the remote sensing perspective, *New Phytol.*, 187, 569–578, <https://doi.org/10.1111/j.1469-8137.2010.03310.x>, 2010.
- Bart, R. R., Kennedy, M. C., Tague, C. L., and McKenzie, D.: Integrating fire effects on vegetation carbon cycling within an ecophysiological model, *Ecol. Model.*, 416, 108880, <https://doi.org/10.1016/j.ecolmodel.2019.108880>, 2020.
- Bowman, D. M., Kolden, C. A., Abatzoglou, J. T., Johnston, F. H., van der Werf, G. R., and Flannigan, M.: Vegetation fires in the Anthropocene, *Nature Reviews Earth & Environment*, 1, 500–515, <https://doi.org/10.1038/s43017-020-0085-3>, 2020.
- Breiman, L.: Random forests, *Mach. Learn.*, 45, 5–32, <https://doi.org/10.1023/A:1010933404324>, 2001.
- Burton, C., Lampe, S., Kelley, D. I., Thiery, W., Hantson, S., Christidis, N., Gudmundsson, L., Forrest, M., Burke, E., Chang, J., Huang, H., Ito, A., Kou-Giesbrecht, S., Lasslop, G., Li, W., Nieradzik, L., Li, F., Chen, Y., Randerson, J., Reyer, C. P. O., and Mengel, M.: Global burned area increasingly explained by climate change, *Nat. Clim. Change*, 14, 1186–1192, <https://doi.org/10.1038/s41558-024-02140-w>, 2024.
- Cansler, C. A. and McKenzie, D.: How robust are burn severity indices when applied in a new region? Evaluation of alternate field-based and remote-sensing methods, *Remote Sensing*, 4, 456–483, <https://doi.org/10.3390/rs4020456>, 2012.
- Collar, N. M., Saxe, S., Rust, A. J., and Hogue, T. S.: A CONUS-scale study of wildfire and evapotranspiration: Spatial and temporal response and controlling factors, *J. Hydrol.*, 603, 127162, <https://doi.org/10.1016/j.jhydrol.2021.127162>, 2021.
- Cooper, C. E., Aparecido, L. M., Muir, J. P., Morgan, C. L., Heilman, J. L., and Moore, G. W.: Transpiration in recovering mixed loblolly pine and oak stands following wildfire in the Lost Pines region of Texas, *Ecophysiology*, 12, e2052, <https://doi.org/10.1002/eco.2052>, 2019.
- DeBano, L. F., Neary, D. G., and Ffolliott, P. F.: Fire effects on ecosystem, John Wiley & Sons, ISBN 978-0-471-16356-5, 1998.
- DeSoto, L., Cailleret, M., Sterck, F., Jansen, S., Kramer, K., Robert, E. M. R., Aakala, T., Amoroso, M. M., Bigler, C., Camarero, J. J., and Čufar, K.: Low growth resilience to drought is related to future mortality risk in trees, *Nat. Commun.*, 11, 545, <https://doi.org/10.1038/s41467-020-14300-5>, 2020.
- Eidenshink, J., Schwind, B., Brewer, K., Zhu, Z. L., Quayle, B., and Howard, S.: A project for monitoring trends in burn severity, *Fire Ecol.*, 3, 3–21, <https://doi.org/10.4996/fireecology.0301003>, 2007.
- Frazier, A. E., Renschler, C. S., and Miles, S. B.: Evaluating post-disaster ecosystem resilience using MODIS GPP data, *Int. J. Appl. Earth Obs.*, 21, 43–52, <https://doi.org/10.1016/j.jag.2012.07.019>, 2013.
- Friedl, M. and Sulla-Menashe, D.: MODIS/Terra+ Aqua Land Cover Type Yearly L3 Global 500 m SIN Grid V061, NASA EOSDIS Land Processes DAAC: Sioux Falls, SD, USA [data set], <https://doi.org/10.5067/MODIS/MCD12Q1.061>, 2022.
- Halofsky, J. E., Peterson, D. L., and Harvey, B. J.: Changing wildfire, changing forests: the effects of climate change on fire regimes and vegetation in the Pacific Northwest, USA, *Fire Ecol.*, 16, 1–26, <https://doi.org/10.1186/s42408-019-0062-8>, 2020.
- Harris, R. M., Remenyi, T. A., Williamson, G. J., Bindoff, N. L., and Bowman, D. M.: Climate–vegetation–fire interactions and feedbacks: trivial detail or major barrier to projecting the future of the Earth system?, *Wires Clim. Change*, 7, 910–931, <https://doi.org/10.1002/wcc.428>, 2016.
- Hersbach, H., Bell, B., Berrisford, P., Hirahara, S., Horányi, A., Muñoz-Sabater, J., and Simmons, A.: The ERA5 global reanalysis, *Q. J. Roy. Meteor. Soc.*, 146, 1999–2049, <https://doi.org/10.1002/qj.3803>, 2020.
- Holling, C. S.: Resilience and stability of ecological systems, *Annu. Rev. Ecol. Syst.*, 4, 1–23, 1973.
- Hu, Z., Yu, G., Fu, Y., Sun, X., Li, Y., Shi, P., Wang, Y., and Zheng, Z.: Effects of vegetation control on ecosystem water use efficiency within and among four grassland ecosystems in China, *Glob. Change Biol.*, 14, 609–1619, <https://doi.org/10.1111/j.1365-2486.2008.01605.x>, 2008.

- Isbell, F., Craven, D., Connolly, J., Loreau, M., Schmid, B., Beierkuhnlein, C., Bezemer, T. M., Bonin, C., Bruehlheide, H., De Luca, E., and Ebeling, A.: Biodiversity increases the resistance of ecosystem productivity to climate extremes, *Nature*, 526, 574–577, <https://doi.org/10.1038/nature15374>, 2015.
- Jin, Y., Randerson, J. T., Goetz, S. J., Beck, P. S., Lorant, M. M., and Goulden, M. L.: The influence of burn severity on postfire vegetation recovery and albedo change during early succession in North American boreal forests, *J. Geophys. Res.-Biogeophys.*, 117, G01036, <https://doi.org/10.1029/2011JG001886>, 2012.
- Jones, M. W., Kelley, D. I., Burton, C. A., Di Giuseppe, F., Barbosa, M. L. F., Brambleby, E., Hartley, A. J., Lombardi, A., Mataveli, G., McNorton, J. R., Spuler, F. R., Wessel, J. B., Abatzoglou, J. T., Anderson, L. O., Andela, N., Archibald, S., Armenteras, D., Burke, E., Carmenta, R., Chuvieco, E., Clarke, H., Doerr, S. H., Fernandes, P. M., Giglio, L., Hamilton, D. S., Hantson, S., Harris, S., Jain, P., Kolden, C. A., Kurvits, T., Lampe, S., Meier, S., New, S., Parrington, M., Perron, M. M. G., Qu, Y., Ribeiro, N. S., Saharjo, B. H., San-Miguel-Ayanz, J., Shuman, J. K., Tanpipat, V., van der Werf, G. R., Veraverbeke, S., and Xanthopoulos, G.: State of Wildfires 2023–2024, *Earth Syst. Sci. Data*, 16, 3601–3685, <https://doi.org/10.5194/essd-16-3601-2024>, 2024.
- Jones, M. W., Smith, A., Betts, R., Canadell, J. G., Prentice, I. C., and Le Quéré, C.: Climate change increases the risk of wildfires, *Science Brief Review*, 116, 117, <https://doi.org/10.5281/zenodo.4746013>, 2020.
- Juang, C. S., Williams, A. P., Abatzoglou, J. T., Balch, J. K., Hurteau, M. D., and Moritz, M. A.: Rapid growth of large forest fires drives the exponential response of annual forest-fire area to aridity in the western United States, *Geophys. Res. Lett.*, 49, e2021GL097131, <https://doi.org/10.1029/2021GL097131>, 2022.
- Juarez-Martinez, E. L., Sprengers, J. J., Cristian, G., Oranje, B., van Andel, D. M., Avramiea, A. E., Simpraga, S., Houtman, S. J., Hardstone, R., Gerver, C., and van der Wilt, G. J.: Prediction of behavioral improvement through resting-state electroencephalography and clinical severity in a randomized controlled trial testing bumetanide in autism spectrum disorder, *Biol. Psychiat.*, 8, 251–261, <https://doi.org/10.1016/j.bpsc.2021.08.009>, 2023.
- Karavani, A., Boer, M. M., Baudena, M., Colinas, C., Díaz-Sierra, R., Pemán, J., de Luis, M., Enríquez-de-Salamanca, Á., and Resco de Dios, V.: Fire-induced deforestation in drought-prone Mediterranean forests: drivers and unknowns from leaves to communities, *Ecol. Monogr.*, 88, 41–169, <https://doi.org/10.1002/ecm.1285>, 2018.
- Koven, C. D., Knox, R. G., Fisher, R. A., Chambers, J. Q., Christoffersen, B. O., Davies, S. J., Detto, M., Dietze, M. C., Faybishenko, B., Holm, J., Huang, M., Kovenock, M., Kueppers, L. M., Lemieux, G., Massoud, E., McDowell, N. G., Muller-Landau, H. C., Needham, J. F., Norby, R. J., Powell, T., Rogers, A., Serbin, S. P., Shuman, J. K., Swann, A. L. S., Varadharajan, C., Walker, A. P., Wright, S. J., and Xu, C.: Benchmarking and parameter sensitivity of physiological and vegetation dynamics using the Functionally Assembled Terrestrial Ecosystem Simulator (FATES) at Barro Colorado Island, Panama, *Biogeosciences*, 17, 3017–3044, <https://doi.org/10.5194/bg-17-3017-2020>, 2020.
- Knauer, J., Zaehle, S., De Kauwe, M. G., Haverd, V., Reichstein, M., and Sun, Y.: Mesophyll conductance in land surface models: effects on photosynthesis and transpiration, *Plant J.*, 101, 858–873, <https://doi.org/10.1111/tpj.14577>, 2020.
- Kumar, N., Singh, H., Kumar, A., Singh, A. K., Pandey, P. K., and Kumar, A.: Forest-Fire-Induced Land Degradation, in: Sustainable Land Management in India, Springer, Singapore, 51–68, <https://doi.org/10.1007/978-981-97-5223-2>, 2024.
- Lasslop, G., Hantson, S., Harrison, S. P., Bachelet, D., Burton, C., Forkel, M., Forrest, M., Li, F., Melton, J. R., Yue, C., and Archibald, S.: Global ecosystems and fire: Multi-model assessment of fire-induced tree-cover and carbon storage reduction, *Glob. Change Biol.*, 26, 5027–5041, <https://doi.org/10.1111/gcb.15160>, 2020.
- Lawrence, D. M., Hurtt, G. C., Arneth, A., Brovkin, V., Calvin, K. V., Jones, A. D., Jones, C. D., Lawrence, P. J., de Noblet-Ducoudré, N., Pongratz, J., Seneviratne, S. I., and Shevliakova, E.: The Land Use Model Intercomparison Project (LUMIP) contribution to CMIP6: rationale and experimental design, *Geosci. Model Dev.*, 9, 2973–2998, <https://doi.org/10.5194/gmd-9-2973-2016>, 2016.
- Li, Y., Shi, H., Zhou, L., Eamus, D., Huete, A., Li, L., Cleverly, J., Hu, Z., Harahap, M., Yu, Q., and He, L.: Disentangling climate and LAI effects on seasonal variability in water use efficiency across terrestrial ecosystems in China, *J. Geophys. Res.-Biogeophys.*, 123, 2429–2443, <https://doi.org/10.1029/2018JG004482>, 2018.
- Lu, J. and Yan, F.: The Divergent Resistance and Resilience of Forest and Grassland Ecosystems to Extreme Summer Drought in Carbon Sequestration, *Land*, 12, 1672, <https://doi.org/10.3390/land12091672>, 2023.
- Marcos, B., Gonçalves, J., Alcaraz-Segura, D., Cunha, M., and Honrado, J. P.: Assessing the resilience of ecosystem functioning to wildfires using satellite-derived metrics of post-fire trajectories, *Remote Sens. Environ.*, 286, 113441, <https://doi.org/10.1016/j.rse.2022.113441>, 2023.
- Mather, J. R. and Yoshioka, G. A.: The role of climate in the distribution of vegetation, *Ann. Assoc. Am. Geogr.*, 58, 29–41, 1968.
- McDowell, N. G., Anderson-Teixeira, K., Biederman, J. A., Breshears, D. D., Fang, Y., Fernandez-de-Una, L., Graham, E. B., Mackay, D. S., McDonnell, J. J., Moore, G. W., and Nehemy, M. F.: Ecological decoupling under changing disturbances and climate, *One Earth*, 6, 251–266, <https://doi.org/10.1016/j.oneear.2023.02.001>, 2023.
- Mills, D., Jones, R., Carney, K., St. Juliana, A., Ready, R., Crimmins, A., Martinich, J., Shouse, K., DeAngelo, B., and Monier, E.: Quantifying and monetizing potential climate change policy impacts on terrestrial ecosystem carbon storage and wildfires in the United States, *Climatic Change*, 131, 163–178, <https://doi.org/10.1007/s10584-014-1118-z>, 2015.
- Myneni, R. B., Hoffman, S., Knyazikhin, Y., Privette, J. L., Glassy, J., Tian, Y., Wang, Y., Song, X., Zhang, Y., Smith, G. R., and Lötters, A.: Global products of vegetation leaf area and fraction absorbed PAR from year one of MODIS data, *Remote Sens. Environ.*, 83, 214–231, [https://doi.org/10.1016/S0034-4257\(02\)00074-3](https://doi.org/10.1016/S0034-4257(02)00074-3), 2002.
- Nolan, R. H., Mitchell, P. J., Bradstock, R. A., and Lane, P. N.: Structural adjustments in resprouting trees drive differences in post-fire transpiration, *Tree Physiol.*, 34, 123–136, <https://doi.org/10.1093/treephys/tpt115>, 2014.
- Parks, S. A. and Abatzoglou, J. T.: Warmer and drier fire seasons contribute to increases in area burned at high severity in west-

- ern US forests from 1985 to 2017, *Geophys. Res. Lett.*, 47, e2020GL089858, <https://doi.org/10.1029/2020GL089858>, 2020.
- Partington, D., Thyer, M., Shanafield, M., McInerney, D., Westra, S., Maier, H., Simmons, C., Croke, B., Jakeman, A.J., Gupta, H., and Kavetski, D.: Predicting wildfire induced changes to runoff: A review and synthesis of modeling approaches, *Wiley Interdisciplinary Reviews: Water*, 9, e1599, <https://doi.org/10.1002/wat2.1599>, 2022.
- Pechony, O. and Shindell, D. T.: Driving forces of global wildfires over the past millennium and the forthcoming century, *P. Natl. Acad. Sci. USA*, 107, 19167–19170, <https://doi.org/10.1073/pnas.1003669107>, 2010.
- Picotte, J. J., Bhattarai, K., Howard, D., Lecker, J., Epting, J., Quayle, B., Benson, N., and Nelson, K.: Changes to the Monitoring Trends in Burn Severity program mapping production procedures and data products, *Fire Ecol.*, 16, 1–12, <https://doi.org/10.1186/s42408-020-00076-y>, 2020.
- Poulos, H. M., Barton, A. M., Koch, G. W., Kolb, T. E., and Thode, A. E.: Wildfire severity and vegetation recovery drive post-fire evapotranspiration in a southwestern pine-oak forest, Arizona, USA, *Remote Sensing in Ecology and Conservation*, 7, 579–591, <https://doi.org/10.1002/rse2.210>, 2021.
- Proença, V., Pereira, H. M., and Vicente, L.: Resistance to wildfire and early regeneration in natural broadleaved forest and pine plantation, *Acta Oecol.*, 36, 626–633, <https://doi.org/10.1016/j.actao.2010.09.008>, 2010.
- Rammer, W., Braziunas, K. H., Hansen, W. D., Ratajczak, Z., Westering, A. L., Turner, M. G., and Seidl, R.: Widespread regeneration failure in forests of Greater Yellowstone under scenarios of future climate and fire, *Glob. Change Biol.*, 27, 4339–4351, <https://doi.org/10.1111/gcb.15726>, 2021.
- Ratajczak, Z., Nippert, J. B., Briggs, J. M., and Blair, J. M.: Fire dynamics distinguish grasslands, shrublands and woodlands as alternative attractors in the Central Great Plains of North America, *J. Ecol.*, 102, 1374–1385, <https://doi.org/10.1111/1365-2745.12311>, 2014.
- Rifai, S. W., De Kauwe, M. G., Gallagher, R. V., Cernusak, L. A., Meir, P., and Pitman, A. J.: Burn severity and post-fire weather are key to predicting time-to-recover from Australian forest fires, *Earth's Future*, 12, e2023EF003780, <https://doi.org/10.1029/2023EF003780>, 2024.
- Rodman, K. C., Veblen, T. T., Andrus, R. A., Enright, N. J., Fontaine, J. B., Gonzalez, A. D., Redmond, M. D., and Wion, A. P.: A trait-based approach to assessing resistance and resilience to wildfire in two iconic North American conifers, *J. Ecol.*, 109, 313–326, <https://doi.org/10.1111/1365-2745.13480>, 2021.
- Running, S. W., Mu, Q., Zhao, M., and Moreno, A.: MODIS global terrestrial evapotranspiration (ET) product (MOD16A2/A3 and year-end gap-filled MOD16A2GF/A3GF) NASA Earth Observing System MODIS Land Algorithm (for collection 6), National Aeronautics and Space Administration, Washington, DC, USA [data set], <https://doi.org/10.5067/MODIS/MOD16A2.006>, 2019.
- Running, S. W., Nemani, R. R., Heinsch, F. A., Zhao, M., Reeves, M., and Hashimoto, H.: A continuous satellite-derived measure of global terrestrial primary productivity: Future science and applications, *BioScience*, 56, 547–560, [https://doi.org/10.1641/0006-3568\(2004\)054\[0547:ACSMOG\]2.0.CO;2](https://doi.org/10.1641/0006-3568(2004)054[0547:ACSMOG]2.0.CO;2), 2004.
- Running, S. W. and Zhao, M.: Daily GPP and annual NPP (MOD17A2H/A3H) and year-end gap-filled (MOD17A2HGF/A3HGF) products NASA Earth Observing System MODIS land algorithm, MOD17 [data set], <https://doi.org/10.5067/MODIS/MOD17A2H.006>, 2019.
- Sadler, J. M., Goodall, J. L., Morsy, M. M., and Spencer, K.: Modeling urban coastal flood severity from crowd-sourced flood reports using Poisson regression and Random Forest, *J. Hydrol.*, 559, 43–55, <https://doi.org/10.1016/j.jhydrol.2018.01.044>, 2018.
- Samanta, A., Knyazikhin, Y., Xu, L., Dickinson, R. E., Fu, R., Costa, M. H., Saatchi, S. S., Nemani, R. R., and Myneni, R. B.: Seasonal changes in leaf area of Amazon forests from leaf flushing and abscission, *J. Geophys. Res.-Biogeo.*, 117, G01015, <https://doi.org/10.1029/2011JG001818>, 2013.
- Saigusa, N., Yamamoto, S., Murayama, S., and Kondo, H.: Inter-annual variability of carbon budget components in an AsiaFlux forest site estimated by long-term flux measurements, *Agr. Forest Meteorol.*, 134, 4–16, <https://doi.org/10.1016/j.agrformet.2005.08.016>, 2005.
- Schoennagel, T., Balch, J. K., Brenkert-Smith, H., Dennison, P. E., Harvey, B. J., Krawchuk, M. A., Mietkiewicz, N., Morgan, P., Moritz, M. A., Rasker, R., and Turner, M. G.: Adapt to more wildfire in western North American forests as climate changes, *P. Natl. Acad. Sci.*, 114, 4582–4590, <https://doi.org/10.1073/pnas.1617464114>, 2017.
- Seidl, R., Schelhaas, M. J., Rammer, W., and Verkerk, P. J.: Increasing forest disturbances in Europe and their impact on carbon storage, *Nat. Clim. Change*, 4, 806–810, <https://doi.org/10.1038/nclimate2318>, 2014.
- Shi, M., Liu, J., Zhao, M., Yu, Y., and Saatchi, S.: Mechanistic processes controlling persistent changes of forest canopy structure after 2005 Amazon drought, *J. Geophys. Res.-Biogeo.*, 122, 3378–3390, <https://doi.org/10.1002/2017JG003966>, 2017.
- Shi, M., McDowell, N. G., Huang, H., Zahura, F., Li, L., Forbes, B., Powers-McCormack, B., and Chen, X.: Data and Scripts associated with a manuscript on ecosystem responses to wildfires in the Columbia River Basin. River Corridor and Watershed Biogeochemistry SFA, ESS-DIVE repository [data set], <https://doi.org/10.15485/2507048>, 2025.
- Shi, M., Parazoo, N. C., Jeong, S. J., Birch, L., Lawrence, P., Euskirchen, E. S., and Miller, C. E.: Exposure to cold temperature affects the spring phenology of Alaskan deciduous vegetation types, *Environ. Res. Lett.*, 15, 025006, <https://doi.org/10.1088/1748-9326/ab6502>, 2020.
- Shrestha, S., Williams, C. A., Rogers, B. M., Rogan, J., and Kulakowski, D.: Divergent biophysical responses of western United States forests to wildfire driven by eco-climatic gradients, *Biogeosciences*, 21, 2207–2226, <https://doi.org/10.5194/bg-21-2207-2024>, 2024.
- Stoy, P. C., El-Madany, T. S., Fisher, J. B., Gentine, P., Gerken, T., Good, S. P., Klosterhalfen, A., Liu, S., Miralles, D. G., Perez-Priego, O., Rigden, A. J., Skaggs, T. H., Wohlfahrt, G., Anderson, R. G., Coenders-Gerrits, A. M. J., Jung, M., Maes, W. H., Mammarella, I., Mauder, M., Migliavacca, M., Nelson, J. A., Poyatos, R., Reichstein, M., Scott, R. L., and Wolf, S.: Reviews and syntheses: Turning the challenges of partitioning ecosystem evaporation and transpiration into opportunities, *Biogeosciences*, 16, 3747–3775, <https://doi.org/10.5194/bg-16-3747-2019>, 2019.

- Sulla-Menashe, D. and Friedl, M. A.: User guide to collection 6 MODIS land cover (MCD12Q1 and MCD12C1) product, USGS: Reston, VA, USA, NASA EOSDIS Land Processes Distributed Active Archive Center [data set], <https://doi.org/10.5067/MODIS/MCD12Q1.006>, 2018.
- Sun, Q., Meyer, W. S., Koerber, G. R., and Marschner, P.: Rapid recovery of net ecosystem production in a semi-arid woodland after a wildfire. *Agr. Forest Meteorol.*, 291, 108099, <https://doi.org/10.1016/j.agrformet.2020.108099>, 2020.
- Turner, M. G.: Disturbance and landscape dynamics in a changing world, *Ecology*, 91, 2833–2849, <https://doi.org/10.1890/10-0097.1>, 2010.
- Turner, M. G., Braziunas, K. H., Hansen, W. D., and Harvey, B. J.: Short-interval severe fire erodes the resilience of subalpine lodgepole pine forests, *P. Natl. Acad. Sci. USA*, 116, 11319–11328, <https://doi.org/10.1073/pnas.1902841116>, 2019.
- Westerling, A. L.: Increasing western US forest wildfire activity: sensitivity to changes in the timing of spring, *Philos. T. R. Soc. B*, 371, 20150178, <https://doi.org/10.1098/rstb.2015.0178>, 2016.
- Williams, A. P., Abatzoglou, J. T., Gershunov, A., Guzman-Morales, J., Bishop, D. A., Balch, J. K., and Lettenmaier, D. P.: Observed impacts of anthropogenic climate change on wildfire in California, *Earth's Future*, 7, 892–910, <https://doi.org/10.1029/2019EF001210>, 2019.
- Wimberly, M. C. and Liu, Z.: Interactions of climate, fire, and management in future forests of the Pacific Northwest, *Forest Ecol. Manag.*, 327, 270–279, <https://doi.org/10.1016/j.foreco.2014.06.026>, 2014.
- Wu, J. and Liang, S.: Assessing terrestrial ecosystem resilience using satellite leaf area index, *Remote Sensing*, 12, 595, <https://doi.org/10.3390/rs12040595>, 2020.
- Xu, L., Samanta, A., Costa, M. H., Ganguly, S., Nemani, R. R., and Myneni, R. B.: Widespread decline in greenness of Amazonian vegetation due to the 2010 drought, *Geophys. Res. Lett.*, 38, L07402, <https://doi.org/10.1029/2011GL046824>, 2011.
- Yang, B., Heagy, L. J., Morgenroth, J., and Elmo, D.: Algorithmic Geology: Tackling Methodological Challenges in Applying Machine Learning to Rock Engineering, *Geosciences*, 14, 67, <https://doi.org/10.3390/geosciences14030067>, 2024.
- Yildirim, M. O., Gok, E. C., Hemasiri, N. H., Eren, E., Kazim, S., Oksuz, A. U., and Ahmad, S.: A machine learning approach for metal oxide-based polymer composites as charge selective layers in perovskite solar cells, *Chem Plus Chem*, 86, 785–793, <https://doi.org/10.1002/cplu.202100196>, 2021.
- Yu, L., Fan, L., Ciais, P., Sitch, S., Fensholt, R., Xiao, X., Yuan, W., Chen, J., Zhang, Y., Wu, X., and Qin, Y.: Carbon dynamics of Western North American boreal forests in response to stand-replacing disturbances, *Int. J. Appl. Earth Obs.*, 122, 103410, <https://doi.org/10.1016/j.jag.2023.103410>, 2023.